Analysis of optical gain threshold in n-doped and tensile-strained germanium heterostructure diodes

M. Prost, M. El Kurdi, F. Aniel, N. Zerounian, S. Sauvage, X. Checoury, F. Bœuf, and P. Boucaud

Citation: Journal of Applied Physics **118**, 125704 (2015); doi: 10.1063/1.4931580
View online: http://dx.doi.org/10.1063/1.4931580
View Table of Contents: http://scitation.aip.org/content/aip/journal/jap/118/12?ver=pdfcov
Published by the AIP Publishing

Analysis of optical gain threshold in n-doped and tensile-strained germanium heterostructure diodes

M. Prost,[1,2] M. El Kurdi,[1] F. Aniel,[1] N. Zerounian,[1] S. Sauvage,[1] X. Checoury,[1] F. Bœuf,[2] and P. Boucaud[1]
[1]*Institut d'Electronique Fondamentale, CNRS Université Paris-Sud, Bâtiment 220, F-91405 Orsay, France*
[2]*STMicroelectronics, Rue Jean Monnet, 38054 Crolles, France*

(Received 26 June 2015; accepted 10 September 2015; published online 24 September 2015)

The optical emission of germanium-based luminescent and/or laser devices can be enhanced by tensile strain and n-type doping. In this work, we study by simulation the interplay between electrical transport and optical gain in highly n-doped and intrinsic germanium p-n heterostructure diodes under tensile strain. The effects of strain and doping on carrier mobilities and energy distribution are taken into account. Whereas the n-doping of Ge enhances the filling of the indirect L and Brillouin zone-center conduction band states, the n-doping also reduces the carrier injection efficiency, which is detrimental for the achievement of optical gain at reduced current densities. For applied biaxial strains larger than 1.25%, i.e., far before reaching the cross-over from indirect to direct band gap regime, undoped germanium exhibits a lower optical gain threshold as compared to doped germanium. We also show that the threshold current needed to reach transparency in germanium heterostructures has been significantly underestimated in the previous works. © *2015 AIP Publishing LLC*. [http://dx.doi.org/10.1063/1.4931580]

I. INTRODUCTION

An efficient optical source operating at room temperature and monolithically integrated on a silicon chip represents a significant challenge for silicon photonics. In this perspective, germanium is an interesting active optical material for integrated photonics with the advantage to be fully compatible with a Si-based processing environment. Up to recent years, the weak radiative emission efficiency of Ge due to its indirect band gap structure has been the main limitation for its integration as an optical source. It has been proposed that this limitation could be overcome by applying tensile strain and/or n-type doping to the material. The tensile strain allows one to decrease the energy difference between indirect and direct conduction bands, thus enabling an enhanced carrier injection in Brillouin zone center where efficient direct optical transitions occur. It has been shown that germanium should exhibit a direct band gap for biaxial tensile strains above 1.7%–1.9%[1] or uniaxial strains above 4.6%.[2] The interest for n-doping and tensile strain in germanium was reinforced by the demonstration of laser emission under electrical injection in n-doped germanium layers directly grown on silicon.[3] In the latter case, a low level of biaxial strain, around 0.25%, was applied by using the difference of thermal expansion coefficients between Si and Ge during the growth, in combination with a n-type doping concentration over $4 \times 10^{19}\,\mathrm{cm}^{-3}$. The level of injected current used for this lasing demonstration is, however, too high (above $300\,\mathrm{kA/cm}^2$) for integration purposes. One of the routes to decrease this current density is to apply a larger tensile strain in Ge. N-doping of germanium is also an interesting approach to overcome the indirect character of the conduction band due to the filling of the indirect band states. The enhancement of the direct band gap emission of germanium by n-doping has been evidenced experimentally both by photoluminescence[4,5] and electroluminescence.[6,7] In a simplified image, the larger the doping, the lower the threshold density. The question is to know whether there is an optimum or a trade-off when combining tensile strain and n-doping. The objective of the work presented below is to answer this question.

Several groups have fabricated luminescent germanium diodes with a successful observation of direct band gap contributions to the emission spectrum.[4,6,8–12] To realize an effective pumping in the n-doped active germanium layer, one should preferentially use double heterostructures (DH) that provide a type-I band alignment for both electrons and holes. The barriers can be formed with III-V materials to obtain lattice-matched interfaces[13] or with Si layers, which is the preferred choice for complementary metal oxide semiconductor (CMOS) process compatibility. A specific study of transport properties in these luminescent or lasing diode heterostructures has not been tackled to our knowledge.[14–16] In this work, we investigate the transport properties in n-doped and tensile-strained germanium and the current threshold required for lasing under electrical injection. For simplicity, we choose to focus on the specific case of Si/Ge/Si double heterostructures. Similar results are expected for SiGe/Ge/SiGe double heterostructures. A realistic modeling of gain spectrum accounting for broadening effects is introduced to calculate the threshold current to reach transparency. It is shown that heterostructures with undoped germanium can have a lower lasing threshold as compared to doped heterostructures even below the transition from indirect to direct band gap material. We note that the strain shifts the laser emission to long wavelength. The proposed devices could either be used as (i) optical sources for silicon photonics links, provided that the operation wavelength of other active devices like detectors is also shifted to long wavelength using the same strain strategies or (ii) silicon-based

emitters for sensing applications in the 2–3 μm spectral range.

II. TRANSPORT MODELING

The transport modeling uses the drift-and-diffusion model with doping dependent carrier mobilities and carrier densities including Shockley-Read-Hall lifetimes (SRH),[17] Auger scattering rates,[18] and optical recombination rates[19] of the different materials. The metallic contacts on the semiconductor barrier layers are set to be perfectly ohmic (i.e., infinite recombination rate at the boundaries with metal). The band diagram of the undoped Si/Ge/Si double heterostructure is shown in Fig. 1(a). The minimum of the conduction band is in the Δ valley for silicon, whereas it is in the L valley for germanium. The valence band offset between silicon and germanium varies between 0.3 and 0.8 eV (Refs. 20–23) depending of the strain configuration. We choose to set the value of the band offset at 0.5 eV. This configuration leads to a type II band alignment where the Si conduction band exhibits an energy minimum in the Δ valley at 0.1 eV below the L valley minimum of the germanium layer. For simplicity, we consider the case of unstrained silicon cladding layers on the top and under the germanium layer. The effect of strain on Si layers is not expected to change significantly the results presented below. Fig. 1(b) shows the band diagram at zero applied bias for the DH considering p and n-type silicon cladding layers with $5 \times 10^{19}\,cm^{-3}$ and $10^{18}\,cm^{-3}$ doping levels, respectively. Despite the initial type II band alignment in the undoped case, the introduction of p and n-type doping in the silicon layers and the n-type doping in the germanium layer leads to the appropriate band alignment, because of the Fermi level alignment between the p and n-type layers. Such configuration confines both electrons and holes in germanium. It is also true when undoped germanium is sandwiched between p-Si and n-Si. Under forward bias and high current injection in Ge, the band bending in the germanium layer vanishes and the conduction band discontinuity is only a fraction of the band bending at the interface. The out-of-equilibrium band alignment leads to electron and hole carrier confinement in germanium. When germanium is heavily n-type doped, the acceptor density for the p-type cladding layer must be higher or equal to the donor density in the germanium layer to ensure a high carrier injection efficiency. As shown in Fig. 2(a) for an applied forward bias of 1 V, the holes injected from the p-type Si cladding layer are blocked by the valence band barrier ΔE_v at the Ge/n-Si interface and can thus recombine with injected electrons in the n-Ge layer. Fig. 2(b) shows the $n \times p$ product of minority carrier densities for 1 V applied bias. The radiative recombination rate is directly linked to this quantity and is rather homogeneous in the Ge layer.

The electron distribution is modeled with a single band approach using the characteristic parameters of the L valley in germanium and Δ valley in silicon. This approach is well justified for silicon, since the Δ valleys are significantly separated from other valleys with splitting energies of 0.88 eV and 2.28 eV with the L and Γ valleys, respectively. In germanium, the electrons' occupation rate in the higher-energy Γ and Δ valleys is considerably low as compared to the one of the L valley. Typically, for unstrained germanium, the fraction of electrons in the Γ valley n_Γ is only 0.01% of the electron density in the L valley n_L.[24] When a tensile strain is applied, the reduction of energy difference between L and Γ valleys leads to an increase of the n_Γ density. The n_Γ/n_L ratio can reach about 2% for 2% biaxial tensile strain. At such high level of strain, germanium exhibits a direct band gap. Despite this direct band gap, the very high density of states of the L valley with respect to the density of states of the Γ valley explains that the n_Γ/n_L ratio remains weak. We can thus assume that the electron distribution is predominantly characterized by the L band parameters and we can neglect the influence of other bands on the electron population. Technology Computer Aided Design (TCAD) with Silvaco ATLAS software is used to simulate the carrier transport. The simulations are then performed assuming a single conduction band with characteristics of silicon Δ valley for the barriers and L valley for germanium, with the assumption of continuity of the carrier transport at the interfaces between lowest energy valleys. Concerning the strain dependence of electron mobility in germanium, Fischetti and Laux have estimated a strong mobility increase when tensile strain is increased.[25] We have thus included the variation of the

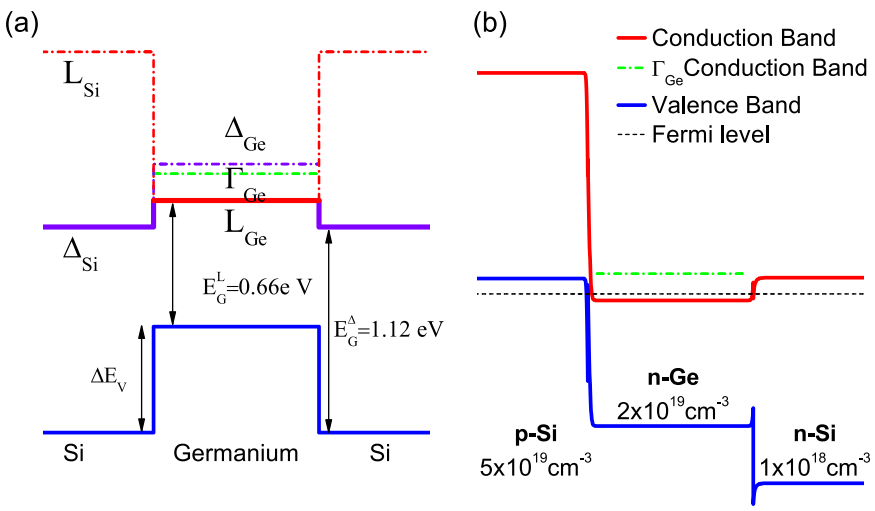

FIG. 1. (a) Band diagram as used for the transport modeling without doping. The blue lines represent the valence band, purple lines are the Δ conduction band, red lines are the L conduction band, and the green one is the Γ conduction band. (b) By introducing doping at equilibrium (0 V applied bias), the black dotted line shows the position of the Fermi level. Only the bands used for carrier transport are represented in continuous lines.

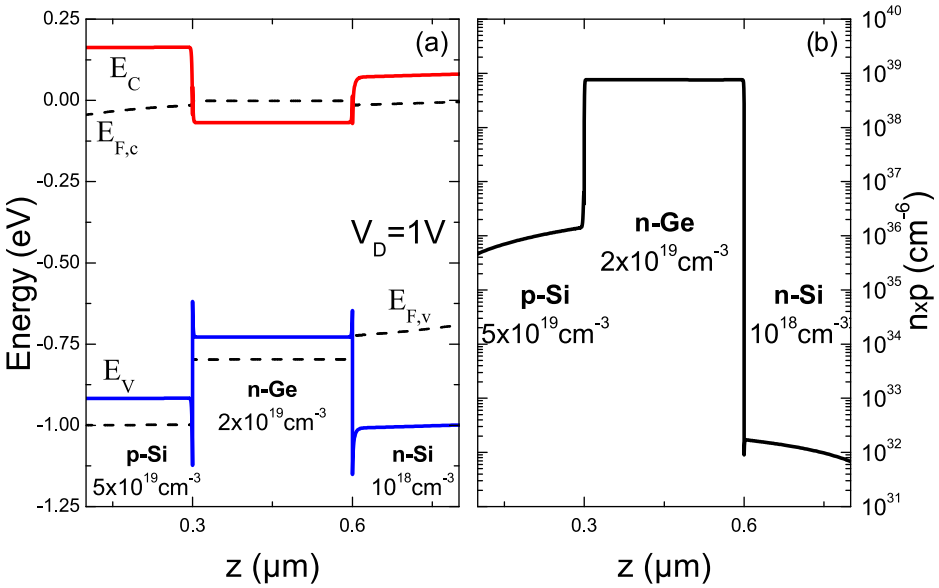

FIG. 2. (a) Band diagram of the double heterostructure and (b) corresponding distribution of n × p product in the germanium layer, under a forward bias of 1 V.

electron mobility with strain in the modeling of the tensile-strained germanium diode characteristics. We consider electron mobility of 3800 $cm^2\ V^{-1}\ s^{-1}$ for unstrained and undoped Ge, which increases up to 9000 $cm^2\ V^{-1}\ s^{-1}$ for 1.5% biaxial tensile strain.[25]

Concerning the hole transport, the situation is different due to the degenerate character of the valence band. For unstrained germanium, since the heavy hole effective mass of density of states is 10 times larger than for the light hole band, we estimate that the light hole population can be neglected and the hole distribution is mainly represented by the heavy hole band parameters when germanium is unstrained. Under tensile strain, this assumption is not fully realistic *a priori*, since tensile strain induces a valence band splitting, the heavy hole band is pushed at lower energy, and the minimum of the valence band energy is given by the light hole band. The carrier distribution between heavy hole and light hole bands depends on the hole density. When the tensile strain is large, the carriers are mostly distributed in the light hole band for small hole densities around $10^{17}\,cm^{-3}$ (90% of carriers for a tensile strain of 2%, for example). But this situation completely changes when increasing the hole density. For a $10^{18}\,cm^{-3}$ hole density, the increase of the valence band quasi-Fermi level energy leads to a stronger heavy hole population that becomes no more negligible and can be equivalent to the light hole population. Thus, to improve the description of hole distributions, we have independently calculated the valence band quasi-Fermi level $E_{F,V}$ as a function of injected hole density for various tensile strains in germanium with a multiband formalism. The results are shown in Fig. 3(a). Note that the filling of the valence band is clearly increased by strain due to the splitting-induced reduction of the valence band density of states. The modeling of hole transport can be performed by considering only one single hole band model. We have performed hole injection modeling in three different configurations: (i) using light hole band parameters for the effective mass of density of states and the mobility, (ii) using heavy hole band parameters for the effective mass of density of states and the mobility, and (iii) using averaged valence band effective masses of density of states such that the hole energy distribution fits the one as obtained from the multiband model of Fig. 3(a). In all cases, as far as carrier injection efficiency is concerned, i.e., injected hole densities versus current density as shown in

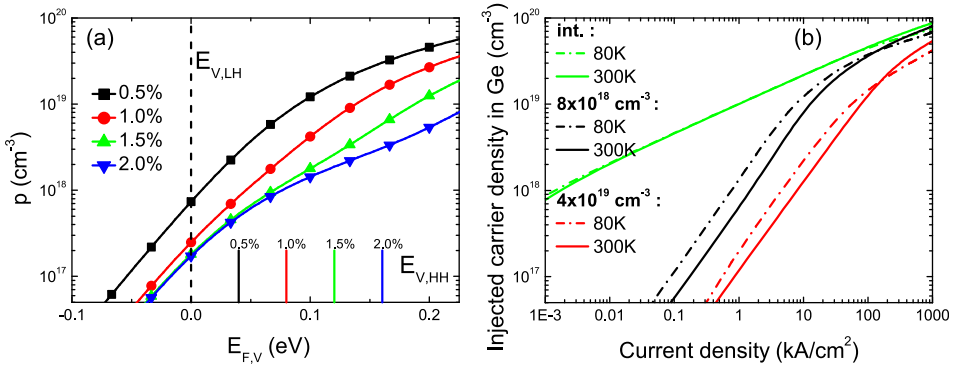

FIG. 3. (a) Total hole density as a function of valence band Fermi level energy $E_{F,V}$ for different applied biaxial tensile strains in germanium. The vertical lines show the position of $E_{V,HH}$ for different tensile strains to illustrate the energy splitting between heavy and light hole valleys. (b) Injected carrier density calculated as a function of the total current density using a double heterostructure p-Si/Ge/n-Si for intrinsic Ge (int) and for n-doped germanium with $N_D = 8 \times 10^{18}\,cm^{-3}$ to $4 \times 10^{19}\,cm^{-3}$ at 80 K and 300 K. The p-type Si layer is doped with $N_A = 5 \times 10^{19}\,cm^{-3}$ and the n-type Si layer is doped with $N_D = 10^{18}\,cm^{-3}$.

Fig. 3(b), the results are similar in the studied range of current densities considered in this work. In the following, we have thus performed the simulations with the heavy hole band parameters, since the hole density can span a wider range as a function of carrier injection. This assumption is also justified by the fact that the results obtained in Fig. 3(a) with a multiband formalism can be well fitted with a single band model with adjusted effective masses, close to the heavy hole mass in most of the cases. The influence of strain on the hole mobility is introduced in the same way as for electron mobility using Fischetti's parameters. Since we did consider the transport perpendicular to the in-plane strain, we use the mobility as defined by μ_{perp} in Ref. 25, μ_{perp} is $1900\,cm^2\,V^{-1}\,s^{-1}$ for unstrained and undoped Ge, and increases up to $7900\,cm^2\,V^{-1}\,s^{-1}$ for 1.5% biaxial tensile strain. We emphasize that the variation of the mobility has a very weak incidence on the modeling of carrier injection efficiency but mostly impacts the diode current-voltage characteristics.

To summarize, the transport modeling is performed by considering a single valence and conduction energy band. We study the carrier filling of the different valleys under electrical injection. We made the hypothesis that the transport is only relevant in the L valley for the conduction band. For valence band, simulations are performed using single heavy hole band parameters with strain-dependent mobilities and we use the results of Fig. 3(a) to obtain a more realistic evaluation of the quasi-Fermi level. As the L valley and heavy hole bands are lowered with the same dynamic as a function of applied strain, the band gap energy $E_G^{L/HH}$ between these two valleys used for the simulation remains constant.

The effect of doping is also introduced in the modeling. N-type doping has been considered as a very interesting approach to increase electron injection in the upper Γ valley and population inversion, when germanium is not sufficiently strained to reach the direct band gap regime. However, it is known that the introduction of doping leads to scattering effects reducing the carrier mobilities and lifetimes.[17,26] The variation of mobilities for electrons and holes *vs.* doping and SRH lifetime reduction are introduced into the transport modeling following the data of Helling *et al.* for germanium.[27] For doped silicon layers, the mobility variation is introduced following the unified model proposed by Klaassen.[28] The SRH lifetime depends on the defect density. For a n-type doping concentration of $N_D = 10^{19}\,cm^{-3}$ in germanium, the SRH minority carrier lifetime is shortened by two orders magnitude as compared to undoped germanium[27] to a value estimated around $\tau_{SRH} = 3\,ns$. Considering an Auger recombination coefficient of $10^{-30}\,cm^6\,s^{-1}$ and a density of excess carrier of $10^{19}\,cm^{-3}$, the Auger lifetime is $\tau_{Aug} = 10\,ns$. The real lifetime must be shorter under high carrier injection regime. With the carrier confinement due to the use of the cladding layers, the charge neutrality is allowed by recombination process in germanium. The injection velocity process of such diodes is thus mainly controlled by the carrier lifetime in the germanium, and the doping has a direct incidence on the resulting current. As can be seen in Fig. 3(b), the n-doping degrades significantly the carrier injection efficiency in germanium for a fixed current, with a much lower injected carrier density when doping is increased. As an example at room temperature, one needs a current density of $13\,kA/cm^2$ to reach an injected carrier density of $10^{19}\,cm^{-3}$ with $N_D = 8 \times 10^{18}\,cm^{-3}$ and $75\,kA/cm^2$ with $N_D = 4 \times 10^{19}\,cm^{-3}$. In undoped germanium, the corresponding current density is only $1\,kA/cm^2$ to reach a carrier injection of $10^{19}\,cm^{-3}$. There is thus a trade-off between the L-band filling effect by doping needed for luminescence improvement and the carrier injection efficiency required to reach certain carrier densities.

We also performed low temperature carrier injection simulations at 80 K. The parameters for simulations are adapted (SRH lifetime, mobility enhancement, and band gap energy variation). The freezing of dopant impurities is not taken into account as we expect that the impact of this effect starts to be important at lower temperature. For low level injection, the current density is reduced by a factor of 2 in the case of n-type germanium layer as compared to 300 K, due to the carrier mobility improvement and quasi-Fermi level position closer to the conduction band in n-type germanium.

III. DETERMINATION OF CURRENT THRESHOLD FOR POPULATION INVERSION

For direct band gap semiconductors, the population inversion criterion is given by the Bernard-Duraffourg relation $E_{F,C} - E_{F,V} > E_G^{\Gamma}$.[29] For germanium that is an indirect band gap semiconductor, we need to adapt this criterion to take into account the indirect L valley. We made the hypothesis that the quasi-Fermi level in the conduction band is fixed by the carrier distribution in the L valley. Consequently, to ensure carrier filling in the direct valley, the quasi-Fermi level must be aligned with the Γ band-edge energy $E_{C,\Gamma}$. The criterion becomes $E_{F,C} - E_{C,L} > E_{C,\Gamma} - E_{C,L}$, where the energy position of quasi-Fermi level $E_{F,C}$ from the L band edge must be higher than the splitting energy between L and Γ. We remind that this splitting energy is dependent on the applied strain. In the same manner, the criterion where $E_{F,V}$ is lower than the valence band edge is also applied for the valence band. The population inversion is obtained when these two criteria are met.

In Fig. 4(a), we show the calculated current threshold for population inversion as a function of strain and doping using the above-mentioned criteria. The curves show a step-like behavior with a threshold current drop by one order of magnitude for a tensile strain increase of only few tenth of %. The position of the current drop depends on the doping. The current drop occurs at tensile strain of 0.75%, 1.1%, and 1.5% for doping levels of $4 \times 10^{19}\,cm^{-3}$, $2 \times 10^{19}\,cm^{-3}$, and $8 \times 10^{18}\,cm^{-3}$, respectively. Before the current drop, the threshold current needed to reach population inversion corresponds to the one needed to satisfy the criterion $E_{F,C} - E_{C,L} > E_{C,\Gamma} - E_{C,L}$ while the strain and doping are not sufficient to allow it by themselves. The required current corresponds to the one needed to fill all L band states at energies lower than the Γ conduction band edge. In this regime, the current threshold diminishes continuously as the applied tensile strain is increased due to the reduction of the L–Γ energy splitting. Above the current drop, the current threshold for

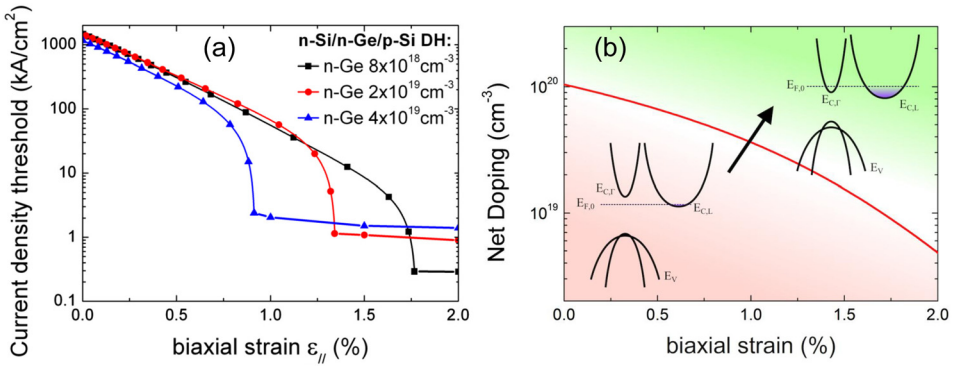

FIG. 4. (a) Calculated threshold current densities for zone-center population inversion in n-doped germanium as a function of applied biaxial strain using a double heterostructure p-Si/Ge/n-Si for various doping levels in the Ge layer. (b) Summarizing view of the dependence of the current threshold drop as a function of doping and strain. The red line gives the separation between two distinct phase regimes. In the red region, the required current density that allows to satisfy $E_{F,C} - E_{C,L} > E_{C,\Gamma} - E_{C,L}$ is very high, while after crossing the red line, one could reach the green region where the combination of tensile strain and doping allows one to significantly decrease the current threshold.

population inversion corresponds to the one needed to attain the situation, where $E_{F,V}$ is higher than the valence band edge. Note that a significant reduction of the current threshold can be obtained by reducing the n-doping but only if the applied tensile strain is sufficiently large. For a 1.75% biaxial tensile strain and a doping level of only $8 \times 10^{18}\,\mathrm{cm}^{-3}$, the current threshold is $290\,\mathrm{A/cm}^2$, much lower than the minimum of current reached for a $4 \times 10^{19}\,\mathrm{cm}^{-3}$ doping, $1.5\,\mathrm{kA/cm}^2$. Shorter lifetimes and mobility degradation with dopant impurities density lead to a higher current density for minority carrier injection in n-type germanium. One can thus decrease the absolute current threshold by reducing the doping only if tensile strain is sufficient to overcome the Γ–L energy splitting. The behavior as given in Fig. 4(a) can be generalized for various doping densities as shown in Fig. 4(b). In Fig. 4(b), we give a schematic view of the threshold current evolution in the two-dimensional strain and doping space of parameters. The red line is separating the two phases, below the current drop (red region) where current threshold is high, and above the current drop (green region) with lower current threshold.

IV. DETERMINATION OF GAIN CURRENT THRESHOLD

Optical gain is calculated using the standard effective mass framework, but taking as input the valence band and conduction band edge energies as obtained from a multiband **k**·**p** formalism.[30–32] The Fermi level in the conduction and in the valence bands are calculated considering also multiband population distribution as done for holes in Fig. 3(a). The gain is calculated by using the following equation:

$$\alpha_{TE,TM}^{HH,LH}(\hbar\omega) = C_0 |D_{HH,LH}^{TE,TM}|^2 \int_0^\infty dE\, \rho_{HH,LH}(E) \times \left[f_c(E) - f_v(E)\right] \times \frac{\frac{\Gamma_0}{2\pi}}{\left(\frac{\Gamma_0}{2}\right)^2 + \left(E_{\Gamma,(HH,LH)} + \mathrm{E} - \hbar\omega\right)^2}. \quad (1)$$

Since the tensile strain induces a splitting of the valence band, one should consider both Γ-HH and Γ-LH transitions at separated energies. This condensed gain formula involves four types of transitions, i.e., Γ-HH and Γ-LH transitions in TE and TM polarizations. We define TE (TM) polarizations as light polarized parallel (perpendicular) to the stress plane. The dipolar matrix elements variation across the germanium layer is calculated using the **k**·**p** formalism as

$$D_{HH,LH}^{TE,TM} = \frac{m_0}{\hbar} \langle u_\Gamma | \vec{\varepsilon} \cdot \vec{\nabla}_k H_{\boldsymbol{k}.\boldsymbol{p}} | u_{\mathrm{HH,LH}} \rangle_{k=0}, \quad (2)$$

where $|u_{\mathrm{HH,LH}}\rangle$ and $|u_\Gamma\rangle$ are the light hole (LH), heavy hole (HH), and Γ zone center Bloch functions at $\mathbf{k} = \mathbf{0}$.

In Eq. (1), $C_0 = \frac{\pi e^2}{n_r c \epsilon_0 m_0^2 \omega}$, where e is the elementary electron charge, n_r is the optical refractive index of germanium, c is the light speed in vacuum, ϵ_0 is the vacuum permittivity, m_0 is the electron mass, $E_{\Gamma,(HH,LH)}$ are direct band gap energies ($E_\Gamma - E_{HH}$ and $E_\Gamma - E_{LH}$), $\hbar\omega$ is the transition energy, f_c and f_v are Fermi statistics distribution, and $\rho_{HH,LH}\left(\hbar\omega - E_{\Gamma,(HH,LH)}\right) = \frac{1}{2\pi^2}\left(\frac{2m_r}{\hbar^2}\right)^{\frac{3}{2}} \sqrt{\hbar\omega - E_{\Gamma,(HH,LH)}}$ are the joint density of states for the Γ and HH bands and the Γ and LH bands with m_r as the reduced effective mass defined by $\frac{1}{m_r} = \frac{1}{m_\Gamma} + \frac{1}{\mathrm{m}_{LH,HH}}$. We use the following effective masses of density of states: $m_{HH} = 0.284\mathrm{m}_0$ ($\mathrm{m}_{LH} = 0.043\mathrm{m}_0$)[33] $m_\Gamma = 0.038\mathrm{m}_0$ ($\mathrm{m}_L = 0.56\mathrm{m}_0$). The carrier interactions with vibrational modes of the crystal (phonon) and scattering effects lead to a homogeneous broadening that can be accounted for by assuming a Lorentzian shape of the transition, and Γ_0 is the full width at half maximum (FWHM) energy of the transition. Note that this spectral broadening introduced in the model induces a decrease of the gain amplitude, since the Lorentzian function is normalized to unity due to the conservation of the transition oscillator strength. In this study, we fixed this value to 30 meV.

The parameters for the wavelength-dependent free-carrier absorption are taken from Ref. 34. The total net gain spectrum is first calculated iteratively accounting for free carrier absorption (FCA) losses, with increasing injected carrier density until its maximum becomes equal to near

zero to deduce the carrier density threshold for material transparency. Then, the current density threshold is obtained by using the transport modeling results as shown in Fig. 3(b) that connect the injected carrier density with total current density. Note that the defined threshold that is presented in this study corresponds to the intrinsic net gain of the material. On the contrary, lasing threshold in real devices occurs when material gain is sufficiently high to overcome cavity losses $\alpha_{cav.}$ For generality, we did consider transparency threshold of the material only, which would be equivalent to the lasing threshold in a lossless optical cavity. The results are summarized in Fig. 5(a) as a function of tensile strain and for different doping levels. As compared to the results shown in Fig. 4(a), one should note that the curves do not exhibit abrupt dependences, with hardly distinguishable current drop at 0.75% tensile strain for $N_D = 4 \times 10^{19}\,cm^{-3}$. The gain calculation uses the carrier distribution functions f_c and f_v and due to energy extension of the distributions with the temperature (i.e., the Fermi function tail due to thermal broadening), allowed transitions involving states at energies above E_{FC} and E_{FV} occur. This contributes to the decrease in the abruptness of the regime transition as obtained for the population inversion threshold (Fig. 4). For the same reason, the effect of doping is not so marked with a relatively low decrease of the threshold when the doping is increased. The gain threshold is only reduced from 471 kA/cm^2 for undoped germanium to 142 kA/cm^2 by introducing n-doping of $4 \times 10^{19}\,cm^{-3}$ at 0.5% biaxial tensile strain. From the results shown in Fig. 5(a), it is clear that undoped germanium will exhibit a lower threshold for strain larger than 1.25% even if the direct band gap regime is not reached for this strain level. The physics mechanism behind this is the following: for unstrained or weakly strained germanium, the population in the Γ valley increases as the doping is increased. There is thus a net advantage to dope germanium. For strains around 1.25–1.5% or higher, the ratio n_Γ/n_L does not increase significantly when doping is increased and even decreases at large strains. Moreover, doping of germanium decreases the non-radiative relaxation time and it thus becomes more difficult to inject a high carrier density in the Ge layer. There is thus no advantage to dope germanium at large strains. Note that when the strain is approaching the onset for indirect-to-direct band gap transition, i.e., such as $E_\Gamma = E_L$ near 1.75% biaxial tensile strain, the gap in threshold widens with a gain threshold of 100 A/cm^2 for undoped germanium versus 1.9 kA/cm^2 for doped germanium up to $4 \times 10^{19}\,cm^{-3}$. Also note that the tensile strain shifts the material gain towards long wavelength. The free carrier absorption introduced by n-doping contributes more heavily to optical losses that must be overcome to reach gain when high tensile strain is applied. If we compare our results from Fig. 5(a) with those reported in other works, we obtain much larger thresholds. Typically, the current threshold reported here is roughly 10 times larger than the one found by Dutt *et al.*[14] For $N_D = 4 \times 10^{19}\,cm^{-3}$, we obtain a current threshold of 26 kA/cm^2 at 1% tensile strain while Dutt *et al.*[14] found a threshold current for gain near 2.4 kA/cm^2. In a previous work,[34] we have calculated the gain threshold by using an equivalent formalism to the one used in Ref. 14, without accounting for broadening of the transition oscillator strength (by taking $\Gamma_0 = 0$). We found a threshold for carrier injection density of $5.8 \times 10^{17}\,cm^{-3}$ for $N_D = 2 \times 10^{19}\,cm^{-3}$, which corresponds to an injected current density of 2.9 kA/cm^2 according to Fig. 3(b). This current threshold is in good agreement with the one found for the same doping density by Dutt *et al.*[14] around 5.1 kA/cm^2. A slight discrepancy between both studies[14,34] could be explained by the choice of the free carrier modeling parameters, the difference in the oscillator strength used to model the absorption of germanium and obviously in the modeling of the transport. From this, we can conclude that the introduction of a more realistic description of the gain accounting for scattering effects that occurs in the material through the broadening Γ_0 is determinant and unfortunately increases noticeably the gain thresholds that have been predicted up to now. We highlight the fact that these scattering mechanisms have usually not been introduced in previous works devoted to gain modeling in germanium, even when high level of n-doping is included in the studies.[35] One should then consider that most of gain values calculated in the literature have been overestimated.[1,15,36,37]

The conclusions given above are slightly different at low temperature. As shown in Fig. 5(b), the gain threshold at 80 K is lower in the high doping level case, $4 \times 10^{19}\,cm^{-3}$, and for biaxial strain below 1.5%. In this regime, germanium still exhibits an indirect band gap and doping allows filling of the indirect band states that is favorable for the reduction of the current threshold for population inversion as discussed in Section III (Fig. 4). Low temperature reduces the energy extension of the carrier distribution, explaining the onset of a drop in current threshold as observed in Fig. 4 at room temperature. The current threshold for samples doped to $4 \times 10^{19}\,cm^{-3}$ is limited to 500 A/cm^2 at 1% of tensile strain

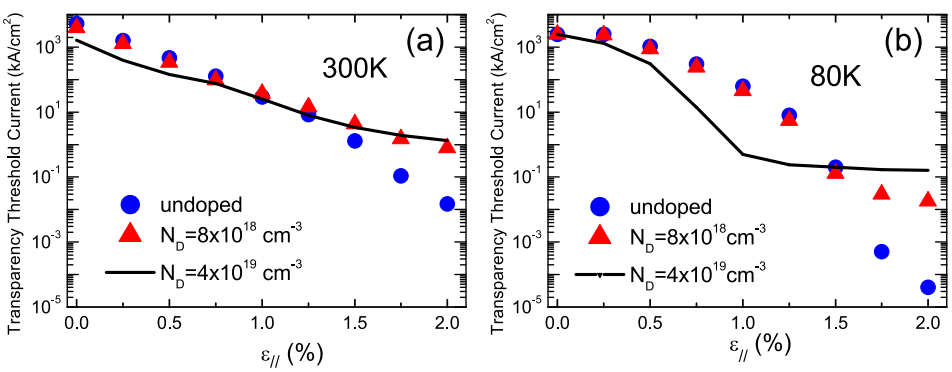

FIG. 5. (a) Calculated threshold current density for transparency as a function of tensile strain, for intrinsic Ge (blue circle) and for n-doped germanium with $N_D = 8 \times 10^{18}\,cm^{-3}$ (red triangle) and $4 \times 10^{19}\,cm^{-3}$ (continuous black line) at 300 K and (b) 80 K.

and decreases slowly with a plateau-like behavior down to 160 A/cm^2 for 2% strain. For biaxial tensile strains larger than 1.5%, the transparency threshold current density is smaller for undoped Ge. The needed current strongly decreases down to 0.5 A/cm^2 and 0.04 A/cm^2 for strains of 1.75% and 2%, respectively, re-enforcing the significance of the tensile strain for gain achievement as compared to doping. For 1.75% and 2% tensile strain, the conduction band splitting E_Γ-E_L reaches 0 meV (indirect to direct band transition point) and −20 meV, respectively. Intrinsic Ge is thus a better option for high performance electrically injected lasers when large tensile strains are present.

V. CONCLUSION

We have studied the effect of n-doping and tensile strain on carrier injection and on optical gain in double heterostructure germanium diodes. There is a competition between the filling effects of the indirect band induced by n-doping that can enhance population inversion and the reduction of injection efficiency induced by the doping. Our results indicate that only a modest improvement to obtain population inversion could be achieved by n-doping, and this improvement occurs solely for low strain regimes where the threshold current remains very large in the hundreds of kA/cm^2 range. Surprisingly, undoped germanium requires a lower current density to reach transparency for biaxial strain level above 1.25%, i.e., well below the cross-over from indirect to direct band gap. Due to the specificity of the electrical injection, heavy doping of Ge is thus not the most efficient way to achieve lasing at room temperature and levels of current density injection compatible with integration. At low temperature, the doping can decrease the transparency threshold for biaxial strain up to 1.5% but is detrimental at higher strain values. With the recent development of enhanced strain transfer methods that leads to quasi-direct band structures, an active region composed of undoped germanium is more favorable to obtain a germanium laser. Our results also predict threshold current densities higher than values previously reported, as a direct consequence of accounting for broadening mechanisms enhanced by doping.

ACKNOWLEDGMENTS

Mathias Prost was funded by an ANRT CIFRE grant. Part of this work was supported by Agence Nationale de la Recherche under GRAAL convention (ANR Blanc call 2011 BS03 00401).

[1]J. Liu, X. Sun, D. Pan, X. Wang, L. C. Kimerling, T. L. Koch, and J. Michel, Opt. Express **15**, 11272 (2007).
[2]D. Nam, D. S. Sukhdeo, S. Gupta, J.-H. Kang, M. L. Brongersma, and K. C. Saraswat, IEEE J. Sel. Top. Quantum Electron. **20**, 1500107 (2014).
[3]R. E. Camacho-Aguilera, Y. Cai, N. Patel, J. T. Bessette, M. Romagnoli, L. C. Kimerling, and J. Michel, Opt. Express **20**, 11316 (2012).
[4]X. Sun, J. Liu, L. C. Kimerling, and J. Michel, Opt. Lett. **34**, 1198 (2009).
[5]M. El Kurdi, T. Kociniewski, T.-P. Ngo, J. Boulmer, D. Debarre, P. Boucaud, J. F. Damlencourt, O. Kermarrec, and D. Bensahel, Appl. Phys. Lett. **94**, 191107 (2009).
[6]M. Schmid, M. Oehme, M. Gollhofer, R. Korner, M. Kaschel, E. Kasper, and J. Schulze, Thin Solid Films **557**, 351 (2014).
[7]S.-L. Cheng, J. Lu, G. Shambat, H.-Y. Yu, K. Saraswat, J. Vuckovic, and Y. Nishi, Opt. Express **17**, 10019 (2009).
[8]M. de Kersauson, R. Jakomin, M. El Kurdi, G. Beaudoin, N. Zerounian, F. Aniel, S. Sauvage, I. Sagnes, and P. Boucaud, J. Appl. Phys. **108**, 023105 (2010).
[9]D. Nam, D. Sukhdeo, S.-L. Cheng, A. Roy, K. Chih-Yao Huang, M. Brongersma, Y. Nishi, and K. Saraswat, Appl. Phys. Lett. **100**, 131112 (2012).
[10]M. Kaschel, M. Schmid, M. Gollhofer, J. Werner, M. Oehme, and J. Schulze, Solid-State Electron. **83**, 87 (2013).
[11]M. Prost, M. El Kurdi, A. Ghrib, X. Checoury, N. Zerounian, F. Aniel, G. Beaudoin, I. Sagnes, C. Baudot, F. Boeuf, and P. Boucaud, Appl. Phys. Lett. **104**, 241104 (2014).
[12]M. Prost, M. El Kurdi, A. Ghrib, S. Sauvage, X. Checoury, N. Zerounian, F. Aniel, G. Beaudoin, I. Sagnes, F. Boeuf, and P. Boucaud, Opt Express **23**, 6722 (2015).
[13]R. Jakomin, M. de Kersauson, M. El Kurdi, L. Largeau, O. Mauguin, G. Beaudoin, S. Sauvage, R. Ossikovski, G. Ndong, and M. Chaigneau, Appl. Phys. Lett. **98**, 091901 (2011).
[14]B. Dutt, D. S. Sukhdeo, D. Nam, B. M. Vulovic, Z. Yuan, and K. C. Saraswat, IEEE Photonics J. **4**, 2002 (2012).
[15]Y. Cai, Z. Han, X. Wang, R. E. Camacho-Aguilera, L. C. Kimerling, J. Michel, and J. Liu, IEEE J. Sel. Top. Quantum Electron. **19**, 1901009 (2013).
[16]H. Wen and E. Bellotti, Phys. Rev. B **91**, 035307 (2015).
[17]E. Gaubas, M. Bauza, A. Uleckas, and J. Vanhellemont, Mater. Sci. Semicond. Process. **9**, 781 (2006).
[18]R. Conradt and J. Aengenheister, Solid State Commun. **10**, 321 (1972).
[19]Y. P. Varshni, Phys. Status Solidi B **19**, 459 (1967).
[20]E. T. Yu, E. T. Croke, D. H. Chow, D. A. Collins, M. C. Phillips, T. C. McGill, J. O. McCaldin, and R. H. Miles, J. Vac. Sci. Technol. B **8**, 908 (1990).
[21]L. Colombo, R. Resta, and S. Baroni, Phys. Rev. B **44**, 5572 (1991).
[22]M. M. Rieger and P. Vogl, Phys. Rev. B **48**, 14276 (1993).
[23]C. G. Van de Walle and R. M. Martin, Phys. Rev. B **34**, 5621 (1986).
[24]A. Ghrib, M. de Kersauson, M. El Kurdi, R. Jakomin, G. Beaudoin, S. Sauvage, G. Fishman, G. Ndong, M. Chaigneau, and R. Ossikovski, Appl. Phys. Lett. **100**, 201104 (2012).
[25]M. V. Fischetti and S. E. Laux, J. Appl. Phys. **80**, 2234 (1996).
[26]R. Geiger, J. Frigerio, M. J. Suess, D. Chrastina, G. Isella, R. Spolenak, J. Faist, and H. Sigg, Appl. Phys. Lett. **104**, 062106 (2014).
[27]G. Hellings, G. Eneman, R. Krom, B. de Jaeger, J. Mitard, A. de Keersgieter, T. Hoffmann, M. Meuris, and K. de Meyer, IEEE Trans. Electron Devices **57**, 2539 (2010).
[28]D. B. M. Klaassen, Tech. Dig. –Int. Electron Devices Meet. **1990**, 357–360.
[29]M. G. A. Bernard and G. Duraffourg, Phys. Status Solidi B **1**, 699 (1961).
[30]M. El Kurdi, G. Fishman, S. Sauvage, and P. Boucaud, J. Appl. Phys. **107**, 013710 (2010).
[31]M. El Kurdi, G. Fishman, S. Sauvage, and P. Boucaud, Phys. Rev. B **68**, 165333 (2003).
[32]S. Richard, F. Aniel, and G. Fishman, Phys. Rev. B **70**, 235204 (2004).
[33]R. N. Dexter, H. J. Zeiger, and B. Lax, Phys. Rev. **104**, 637 (1956).
[34]P. Boucaud, M. El Kurdi, A. Ghrib, M. Prost, M. de Kersauson, S. Sauvage, F. Aniel, X. Checoury, G. Beaudoin, and L. Largeau, Photonics Res. **1**, 102 (2013).
[35]A. Ghrib, M. El Kurdi, M. Prost, S. Sauvage, X. Checoury, G. Beaudoin, M. Chaigneau, R. Ossikovski, I. Sagnes, and P. Boucaud, Adv. Opt. Mater. **3**, 353 (2015).
[36]M. Virgilio, C. L. Manganelli, G. Grosso, G. Pizzi, and G. Capellini, Phys. Rev. B **87**, 235313 (2013).
[37]M. de Kersauson, M. El Kurdi, S. David, X. Checoury, G. Fishman, S. Sauvage, R. Jakomin, G. Beaudoin, I. Sagnes, and P. Boucaud, Opt. Express **19**, 17925 (2011).